Journal of Computational Physics 438 (2021) 110370

Contents lists available at ScienceDirect

Journal of Computational Physics

www.elsevier.com/locate/jcp

Discontinuous bubble immersed finite element method for Poisson-Boltzmann-Nernst-Planck model

In Kwon [a], Do Y. Kwak [b,1], Gwanghyun Jo [c,*,2]

[a] Samsung electronics Semiconductor R & D center, Samsungjeonja-ro, Hwaseong-si, Gyeonggi-do, Republic of Korea
[b] Department of Mathematical Science, KAIST, Daejeon, Republic of Korea
[c] Department of Mathematics, Kunsan National University, Gunsan-si, Jeollabuk-do, Republic of Korea

ARTICLE INFO

Article history:
Available online 22 April 2021

Keywords:
Poisson-Boltzmann-Nernst-Planck model
Biomolecular electrostatics
Immersed finite element method
Discontinuous bubble function
Gummel's iteration

ABSTRACT

We develop a numerical scheme for Poisson-Boltzmann-Nernst-Planck (PBNP) model. We adopt Gummel's method to treat the nonlinearity of PBNP where Poisson-Boltzmann equation and Nernst-Planck equation are iteratively solved, and then the idea of discontinuous bubble (DB) to solve the Poisson-Boltzmann equation is exploited [6]. First, we regularize the solution of Poisson-Boltzmann equation to remove the singularity. Next, we introduce the DB function as in [6] to treat the nonhomogeneous jump conditions of the regularized solution. Then, we discretize the discontinuous bubble and the bilinear form of Poisson-Boltzmann equation and solve the discretized linear problem by the immersed finite element method. Once Poisson-Boltzmann equation is solved, we apply the control volume method to solve Nernst-Planck equation via an upwinding concept. This process is repeated by updating the previous approximation until the total residual of the system decreases below some tolerance. We provide our numerical experiments. We observe optimal convergence rates for the concentration variable in all examples having analytic solutions. We observe that our scheme reflects well without oscillations the effect on the distribution of electrons caused by locating the singular charge close to the interface.

© 2021 Elsevier Inc. All rights reserved.

1. Introduction

Predicting behaviours of ion interaction and electrostatic potential plays important roles in many fields such as biological systems, nanofluidic systems and semiconductor devices (see [45,1,15,19,29,13] and references therein). The Poisson-Nernst-Planck (PNP) model is a well established theory for predicting ion transport phenomenon for chemical physical and biological systems [12,19,5]. In a PNP system, one considers all the ion species in a system to describe electrostatic interactions precisely, which results in a large number of equations. Thus, in the presence of multiple ion species, simulating PNP model can be computationally demanding. To reduce the number of equations, Zheng and Wei [49] proposed a new model by combining PNP model and Poisson Boltzmann (PB) model, naming their model PBNP. For the ions of interest, the Nernst-Planck equation is used and for the rest ions, Boltzmann distributions of the total potential are used.

* Corresponding author.
E-mail address: gwanghyun@kunsan.ac.kr (G. Jo).

[1] Second author is supported by the National Research Foundation of Korea (NRF) grant funded by the Korea government (MSIT) (No. 2021R1A2C1003340).
[2] Third author is supported by the National Research Foundation of Korea (NRF) grant funded by the Korea government (MSIT) (No. 2020R1C1C1A01005396).

https://doi.org/10.1016/j.jcp.2021.110370
0021-9991/© 2021 Elsevier Inc. All rights reserved.

Let us describe some of the difficulties arising when solving PBNP equation numerically. First, the coefficients of partial differential equations (PDEs) change abruptly across some interfaces. For example, the dielectric parameter for the potential variable is discontinuous across the solute-solvent interface, and the diffusion coefficient for the ion concentration varies between the channel region and the bulk region. Second, the right side of the PB equation describing the potential variable is represented by the distribution of the Dirac-delta functions. To avoid non-physical solutions, one must carefully regularize the equation. One of the strategies is to subtract the Green's function in solute region from the PB equation to remove the singular terms [9,8,34]. However, nonhomogeneous jump conditions appear due to this subtraction and some approaches to deal with the jump conditions are introduced in [9,8,34]. Third, the electrostatic potential and ion concentration are nonlinear related. Thus, one needs to linearize the system using Newton-Krylov iterations [48] or Gummel's iteration [23, 49,7].

When solving problems with interfaces, a natural approach is to use numerical methods based on fitted grids to overcome the discontinuity of the parameters in a PDE. However, some new approaches which use structured girds for the interface problems were developed recently in FEM community. Extended finite element method (XFEM) [47,4,37,46,10] is one of the efficient methods to solve for interface/crack problems based on uniform grids. The additional basis functions constructed by truncating the shape function along the interfaces are added to the trial/test spaces. Thus, the number of degrees of freedom increase near the interface.

Immersed finite element methods (IFEMs), introduced by Z. Li et al. [39,38], is another type of uniform grids based methods for the interface problems. In IFEM type methods, basis functions are modified to satisfy the local flux continuity condition across the interfaces, so that no extra degrees of freedom are needed near the interface. Since the data structure of the discretized system is simple, efficient solvers can be applied for IFEM, like multigrid methods [16,27]. The error estimates for IFEMs were developed in [39,38,11,33,28] for the elliptic interface problems and in [30,24,25] for the elasticity problems. Also, IFEMs have been applied to various problems, including Robin type elliptic problems [32], multiphase flows in porous media [26], and elasticity problem with spring type nonhomogeneous jump condition [36], and PB equation [34]. Among them, discontinuous bubble-IFEM (DB-IFEM) is effective to solve PDEs with nonhomogeneous jump conditions [6]. In this method, a piecewise discontinuous linear function, called discontinuous bubble (DB) is constructed so as to satisfy the nonhomogeneous jump conditions. By substituting the DB, one obtains homogeneous systems which can be effectively solved by plain IFEM schemes. DB-IFEM and their variants were successfully applied to solve the elasticity problem with spring type jump condition [36] and the nonhomogeneous problem arising from regularization process of PB equation [34].

In this work, we develop DB-IFEM based numerical methods for PBNP model whose process we ketch below. To linearize the systems, we adopt the idea of Gummel's map as in [23,49,7], i.e., the potential variable and the concentration variable are solved sequentially until the total residual of the system decreases below a certain tolerance. To solve for the potential variable, the PB equation is regularized by the subtraction of some Green's functions. After the Green's functions are subtracted, the regularized PDE with nonhomogeneous jump conditions across the solvent-solute region is obtained. The discontinuous bubble satisfying the nonhomogeneous jump conditions is subtracted followed by the IFEM scheme for the homogeneous part of the regularized potential. Thus, potential variable is obtained by the sum of Green's functions, discontinuous bubbles and the IFEM solution of the regularized potential. Next, concentration variable is solved in solute region. To avoid the non-physical solution such as blow up near the channel and bulk interface due to the convection dominated terms, we use the control volume methods together with the upwinding concept as in [3,17,14,2]. Above process is repeated until the some tolerance criteria are reached. We test our schemes to some sample examples having analytic solutions where we observe the optimal convergence rates.

The rest of the paper is organized as follows. The governing equation of PBNP is described in Section 2. In Section 3, we introduce Gummel's scheme based formulation for PBNP model. In Section 4, we develop DB-IFEM for PBNP equation. The numerical experiments are given in Section 5. The conclusion follows in Section 6.

2. Poisson-Boltzmann-Nernst-Planck model

In this section, we explain PBNP model which was introduced to solve PNP equation with a large number of ion species [42,49]. The difficulty lies in the fact that every charged ion species need to be treated as a non-equilibrium diffusive species in the electric field. However, when a charged particle (for example a molecule) undergoes a diffusion-reaction process governed by Nernst-Planck equation in the background electrolyte, the ions of electrolyte can be considered as a quasi-equilibrium state. For example, it can be used for diffusion-controlled enzyme reaction rate calculations [42].

We consider an open domain $\Omega \subset \mathbb{R}^2$, $\Omega = \Omega_m \cup \Omega_s$, where Ω_m represents the solute region (or the ion exclusion region) and Ω_s represents the solvent region (or the ion inclusion region) (see Fig. 1). Γ represents the interface such that $\Gamma = \overline{\Omega_m} \cap \overline{\Omega_s}$. We assume Γ is a C^1-curve. We assume that the total number of ion species in the system is N_c. We choose certain ion species from the whole system and call them ion target species. Although we are not interested in the rest of the ion species, we have to reflect the impact of them on the system. We denote $n_\alpha (\alpha = 1, 2, ..., N_{NP})$ to be the concentration of the target ion species, $n_\beta (\beta = N_{NP} + 1, ..., N_c)$ to be the concentration of the remaining ion species in the system. Then we obtain the following equation for electrostatic potential Φ:

$$-\nabla \cdot (\epsilon \nabla \Phi) = 4\pi \rho_f + 4\pi \sum_{\alpha=1}^{N_{NP}} q_\alpha n_\alpha + 4\pi \sum_{\beta=N_{NP}+1}^{N_c} q_\beta n_\beta, \tag{2.1}$$

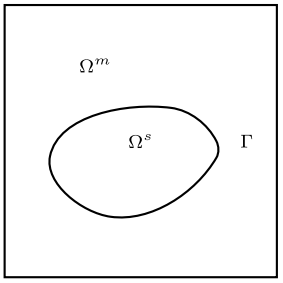

Fig. 1. Domain Ω with interface Γ.

where static charge sources and quasi-equilibrium charge sources are represented respectively by

$$\rho_f = \sum_{j=1}^{N_\alpha} q_j \delta(\mathbf{r} - \mathbf{r}_j),$$
$$n_\beta = n_{0\beta} \exp\left[-\left(q_\beta \Phi - \mu_\beta\right)/k_B T\right].$$

Here, K_B and T are Boltzmann constant and the absolute temperature. We denote $n_{0\beta}$ to be the bulk concentration of the βth ion species, q_α and q_β to be the valence of the αth and βth ion species respectively. $\delta(\mathbf{x})$ is Dirac delta function with q_j being the charge of the biomolecule at position $\mathbf{r}_j (j = 1, 2, ..., N_a)$. N_a indicates the total number of charged atoms in the solute and μ_β is the total chemical potential of βth ion species. The dielectric function ϵ is defined as a piecewise constant function

$$\epsilon(\mathbf{r}) := \begin{cases} \epsilon_m, & \mathbf{r} \in \Omega_m \\ \epsilon_s, & \mathbf{r} \in \Omega_s. \end{cases}$$

Here ϵ_m and ϵ_s represents the dielectric constants in the molecular and solvent regions, respectively. On the other hand, the concentration n_α is governed by the following Nernst-Planck equation:

$$\frac{\partial n_\alpha}{\partial t} = \nabla \cdot \left[D_\alpha \left(\nabla n_\alpha + \frac{q_\alpha n_\alpha}{k_B T} \nabla \Phi \right) \right], \quad \alpha = 1, 2, ..., N_{NP}, \tag{2.2}$$

where $D_\alpha(\mathbf{r})$ is the spatially dependent diffusion coefficient of ion species α. Equations (2.1) and (2.2) are coupled to each other and form a closed equation system. We called the closed equation system the Poisson-Boltzmann-Nernst-Planck equations. The steady state of the equation system (2.1) and (2.2) can be obtained as follows:

$$-\nabla \cdot (\epsilon \nabla \Phi) = 4\pi \rho_f + 4\pi \sum_{\alpha=1}^{N_{NP}} q_\alpha n_\alpha + 4\pi \sum_{\beta=N_{NP}+1}^{N_c} q_\beta n_{0\beta} \exp[-(q_\beta \Phi - \mu_\beta)/(k_B T)], \tag{2.3}$$

$$\nabla \cdot \left[D_\alpha \left(\nabla n_\alpha + \frac{q_\alpha n_\alpha}{\kappa_B T} \nabla \Phi \right) \right] = 0, \quad \alpha = 1, 2, ..., N_{NP}. \tag{2.4}$$

In PBNP system, we describe the ion of interest by the Nernst-Planck model and the others by Boltzmann distribution. Since in the original PNP model we have to solve one Nernst-Planck equation for each ion species, PBNP model can reduce the computational cost when there are multiple ion species in a bimolecular system. Note that Nernst-Planck model is defined only in the solvent domain Ω_s. Zero flux condition is imposed on the interface Γ and each side of the domain. Since (2.1) and (2.2) are coupled each other, the variables Φ and n_α need to be solved iteratively. For the simplicity, we assume that $N_{NP} = N_B = 1$, and define $\psi = \Phi/(k_B T)$, $\gamma = 4\pi/(k_B T)$, and $U_\alpha = \mu_\alpha/(k_B T)$. Then the coupled equations (2.3) and (2.4) are converted into following simpler forms:

$$-\nabla \cdot (\epsilon \nabla \psi) = \gamma [\rho_f + q_1 n_1 + q_2 n_{02} e^{-(q_2 \psi - U_2)}], \tag{2.5}$$

$$-\nabla \cdot [D_1 (\nabla n_1 + q_1 n_1 \nabla \psi)] = 0. \tag{2.6}$$

3. Formulation

In this section, we describe the formulation of PBNP based on Gummel's scheme where PB and NP equations are solved sequentially. First, PB equation is regularized by subtracting some Green's functions, resulting in a PDE with nonhomogeneous jump conditions. Then, by constructing the discontinuous bubble functions, regularized PB equation can be described by weak forms in a continuous space. Finally, linearized NP equation is solved.

The domain of the ion channeling is described in Fig. 2.

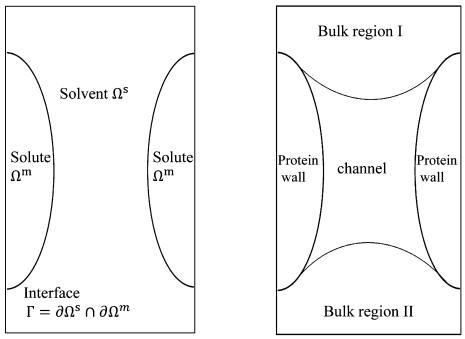

Fig. 2. An illustration of a domain for an ion channeling simulation. Solvent region Ω^s and solute region Ω^m are separated by Γ (left). In particular, a solute region consists of protein walls and solvent region consists of bulk region I, bulk region II, and channel (right).

3.1. Gummel's scheme

Since (2.5)-(2.6) are nonlinear equations of variables ψ and n_1, we need a linearized iterative procedure. We provide the scheme introduced by Gummel [20,49]: Starting from a proper initial guess $\psi^{(0)}$ and $n_1^{(0)}$, $n_1^{(1)}$ can be obtained by solving

$$-\nabla \cdot [D_1(\nabla n_1^{(1)} + q_1 n_1^{(1)} \nabla \psi^{(0)})] = 0. \tag{3.1}$$

Next, $\psi^{(1)}$ is obtained by

$$-\nabla \cdot (\epsilon \nabla \psi^{(1)}) = \gamma[\rho_f + q_1 n_1^{(1)} + q_2 n_{02} e^{-(q_2 \psi^{(0)} - U_2^{(1)})}].$$

Here, the superscript of ψ and n_1 denotes the iteration step. ψ are updated at the jth iteration step as follows:

$$-\nabla \cdot (\epsilon \nabla \psi^{(j)}) + c_{add} \psi^{(j)} = \gamma[\rho_f + q_1 n_1^{(j)} + q_2 n_{02} e^{-(q_2 \psi^{(j-1)} - U_2^{(j)})}] + c_{add} \psi^{(j-1)}, \tag{3.2}$$

where

$$c_{add} = \gamma[q_1 n_1^{(j)} + q_2 n_{02} e^{-(q_2 \psi^{(j-1)} - U_2^{(j)})}].$$

In Gummel's iteration, equations (3.1) and (3.2) are solved iteratively until the stopping criteria is satisfied. During the iteration, U_2 can be obtained by following the [49] way:

$$U_1^{(j)} = \ln(n_1^{(j)}/n_{01}) + q_1 \psi^{(j-1)},$$
$$U_2^{(j)} = a U_1^{(j)} + E_{12},$$

where a, E_{12} are constants taking account of the chemical property of different ions.

3.2. Regularization of PB equation

Before we regularize the solution of PB equation (3.2), we need to describe some function spaces and their norms. From now on, we represent the solvent region as Ω^+, and the solute region as Ω^- for convenience. For any bounded subdomain $D \subset \Omega$, we denote $D^+ = D \cap \Omega^+$, $D^- = D \cap \Omega^-$. We define $H^m(D), H_0^1(D)$ to be the standard Sobolev spaces of order m with the norm $\|\cdot\|_{m,D}$ and the semi-norm $|\cdot|_{m,D}$. For $m = 1, 2$, the space $\widetilde{H}^m(D)$ is defined as

$$\widetilde{H}^m(D) := H^m(D^+) \cap H^m(D^-),$$

with norms

$$\|\psi\|^2_{\widetilde{H}^m(D)} := \|\psi\|^2_{H^m(D^+)} + \|\psi\|^2_{H^m(D^-)}.$$

The subspace $\widetilde{H}_0^1(D)$ is defined as

$$\widetilde{H}_0^1(D) := \{\psi \in \widetilde{H}^1(D) \,|\, \psi = 0 \quad \text{on } \partial D\}$$

Since PB equation has a Dirac delta type singularity, its solution has a logarithmic singularity. It is well known [8] that the solution of PB equation does not belong to $H^1(\Omega)$. So we shall decompose the original solution ψ into a regular solution ψ^r and a singular part ψ^s which takes care of singularities [9].

$$\psi = \psi^r + \psi^s. \tag{3.3}$$

Then, we obtain another equation for the regular solution u^r from the original equation. There are many choices of ψ^s. Among them, we choose the following function:

$$\begin{aligned}\psi^s &= G|_{\Omega^-} \quad \text{in} \quad \Omega^-,\\ \psi^s &= 0 \qquad \text{in} \quad \Omega^+,\end{aligned}$$

where G is defined by $G = -\sum_{i=1}^{N_a} \frac{\gamma q_i}{2\pi\epsilon^-}\log|\mathbf{x}-\mathbf{x}_i|$ in $\mathbb{R}^2$ so that $-\epsilon^-\triangle G = \gamma\rho^f$. Using this choice of ψ^s and (3.3), we obtain the following equation for the regular potential ψ^r from the original equation.

$$-\nabla\cdot(\epsilon\nabla\psi^r) = \gamma[q_1 n_1 + q_2 n_{02} e^{-(q_2\psi^r - U_2)}] \quad \text{in} \quad \Omega, \tag{3.4a}$$

$$[\psi^r]_\Gamma = J_1 \quad \text{on} \quad \Gamma, \tag{3.4b}$$

$$\left[\epsilon\frac{\partial\psi^r}{\partial\mathbf{n}_\Gamma}\right]_\Gamma = J_2 \quad \text{on} \quad \Gamma, \tag{3.4c}$$

$$\psi^r = 0 \quad \text{on} \quad \partial\Omega, \tag{3.4d}$$

where $J_1 = -\psi^s$ and $J_2 = -\epsilon^-\frac{\partial\psi^s}{\partial\mathbf{n}_\Gamma}$. We note that the similar technique of subtracting Green functions to regularize the equation is introduced in [43]. The difference is that Green function in [43] has support on the whole domain while we restrict the support only on Ω^-. The good thing about Green function with smaller support is that, we can reduce the nonlinearity in the Gummel's iteration. We may assume that the equation has homogeneous Dirichlet boundary condition for the convenience. Since the solution of (3.4) satisfies jump conditions, we have to define an affine space where jump conditions are imposed. We introduce $\mathcal{U}_{J_1,J_2}(\Omega)$ as follows:

$$\mathcal{U}_{J_1,J_2}(\Omega) := \{\,\psi\in\widetilde{H}^2(\Omega)\,|\,[\psi]_\Gamma = J_1 \text{ and } \left[\epsilon\frac{\partial\psi}{\partial\mathbf{n}_\Gamma}\right]_\Gamma = J_2 \quad \text{on}\,\Gamma\}.$$

There are a few numerical methods for PB equation using different regularization schemes. For example, jump condition capturing scheme (JCCS) was introduced in [18,9]. JCCS requires an additional harmonic function to remove the jump condition. However, we provide the regularization scheme introduced in [34]. It does not need an additional auxiliary function to treat the jump conditions. Instead, we treat the jump in the solution and flux jumps at once using the DB-IFEM. It is accurate and simple to implement compared with other schemes.

3.3. Weak formulation with DB for nonhomogeneous jumps

We will apply DB scheme introduced in [6] to treat the nonhomogeneous jumps. We apply the regularization scheme to (3.2) and multiply $v\in H_0^1(\Omega)$ on each side of the equation. Applying Green's theorem to each subdomain Ω^+ and Ω^-, we obtain

$$\begin{aligned}&-\int_{\partial\Omega^i}\epsilon\frac{\partial\psi^r}{\partial\mathbf{n}}v\,ds + \int_{\Omega^i}\epsilon\nabla\psi^r\cdot\nabla v\,d\mathbf{x} + \int_{\Omega^i}c_{add}\psi^r v\,d\mathbf{x}\\ &= \int_{\Omega^i}(\gamma[q_1 n_1^{(j)} + q_2 n_{02} e^{-(q_2\psi^{r,(j-1)} - U_2^{(j)})}] + c_{add}\psi^{r,(j-1)})v\,d\mathbf{x}, \quad \forall v\in H_0^1(\Omega),\end{aligned}$$

where $\mathbf{n}$ is the unit outward normal vector to Ω^i ($i=+\text{or}-$). Adding two equations for $i=+,-$ and using (3.4c), we obtain the following:

$$\begin{aligned}&\sum_{i=+,-}\left(\int_{\Omega^i}\epsilon\nabla\psi^r\cdot\nabla v d\mathbf{x} + \int_{\Omega^i}c_{add}\psi^r v\,d\mathbf{x}\right)\\ &= \int_\Gamma J_2 v ds + \sum_{i=+,-}\int_{\Omega^i}\left(\gamma[q_1 n_1^{(j)} + q_2 n_{02} e^{-(q_2\psi^{r,(j-1)} - U_2^{(j)})}] + c_{add}\psi^{r,(j-1)}\right)v\,d\mathbf{x},\ \forall v\in H_0^1(\Omega).\end{aligned} \tag{3.5}$$

Hence we obtain the weak form of (3.4) as follows: Find $\psi^r\in\widetilde{H}^2(\Omega)\cap H_0^1(\Omega)$ satisfying (3.5) and (3.4b). However, the solution of the equation belongs to the affine space $\mathcal{U}_{J_1,J_2}(\Omega)$. We need to treat the nonhomogeneous jumps of the solution to work on a linear space. In order to remove the jumps, we subtract a function defined on a thin strip, called S_Γ, containing Γ (see Fig. 3). We define a *bubble function* ψ^* in $\widetilde{H}^2(S_\Gamma)\cap\widetilde{H}_0^1(S_\Gamma)$ satisfying

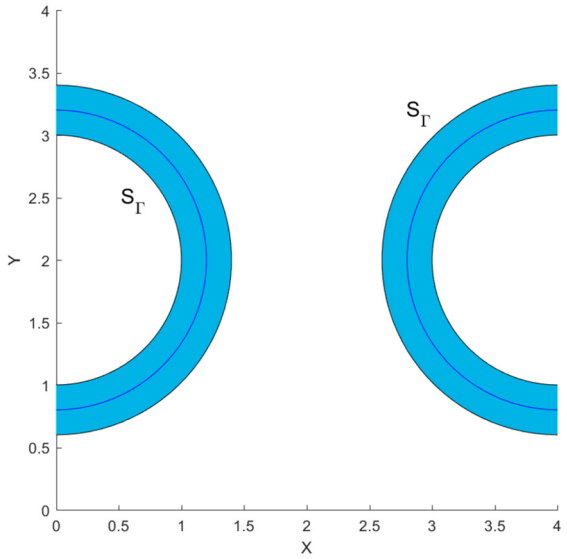

Fig. 3. The shape of S_Γ.

$$[\psi^*] = J_1,$$
$$\left[\epsilon \frac{\partial \psi^*}{\partial \mathbf{n}_\Gamma}\right]_\Gamma = J_2.$$

We let $\bar{\psi} = \psi^r - \psi^*$. Then we easily see that $\bar{\psi} \in H_0^1(\Omega)$. Also, we obtain the equation for $\bar{\psi}$:

$$-\nabla \cdot (\epsilon \nabla \bar{\psi}) + c_{add}\bar{\psi} = \nabla \cdot (\epsilon \nabla \psi^*) + \gamma [q_1 n_1^{(j)} + q_2 n_{02} e^{-(q_2(\bar{\psi}^{(j-1)}+\psi^*)-U_2^{(j)})}] + c_{add}\bar{\psi}^{(j-1)} \quad \text{in } \Omega \setminus \Gamma, \tag{3.6a}$$
$$[\bar{\psi}]_\Gamma = 0 \quad \text{on } \Gamma, \tag{3.6b}$$
$$\left[\epsilon \frac{\partial \bar{\psi}}{\partial \mathbf{n}_\Gamma}\right]_\Gamma = 0 \quad \text{on } \Gamma, \tag{3.6c}$$
$$\bar{\psi} = 0 \quad \text{on } \partial\Omega. \tag{3.6d}$$

Hence, the weak form for $\bar{\psi}$ is as follows: Find $\bar{\psi} \in H_0^1(\Omega)$ satisfying

$$\sum_{i=+,-} \left(\int_{\Omega^i} \epsilon \nabla \bar{\psi} \cdot \nabla v d\mathbf{x} + \int_{\Omega^i} c_{add}\bar{\psi} v d\mathbf{x} \right) = \sum_{i=+,-} \int_{\Omega^i} -\epsilon \nabla \psi^* \cdot \nabla v d\mathbf{x} + \int_\Gamma J_2 v ds$$
$$+ \sum_{i=+,-} \int_{\Omega^i} \left(\gamma [q_1 n_1^{(j)} + q_2 n_{02} e^{-(q_2(\bar{\psi}^{(j-1)}+\psi^*)-U_2^{(j)})}] + c_{add}\bar{\psi}^{(j-1)} \right) v d\mathbf{x}, \tag{3.7}$$

for all v in $H_0^1(\Omega)$.

3.4. Reconstruction of concentration variable

In the previous subsections, in the j-th iteration step electrostatic potential variables are obtained via the method described above. The resulting potential variable at j-th step is obtained as the sum of 1) the solution $\bar{\psi}$ of (3.7), 2) bubble function ψ^*, and 3) Green's function, i.e.,

$$\psi^{(j)} = \bar{\psi} + \psi^* + \sum_{i=1}^{N_a} \left(-\frac{\gamma q_i}{2\pi\epsilon} \log|\mathbf{x} - \mathbf{x}_i| \right).$$

In this subsection, we show how the concentration of the ion is updated. We solve the following linearized Nernst-Planck equation:

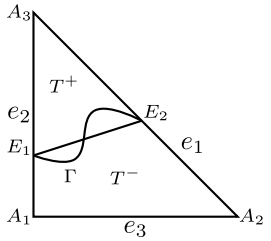

Fig. 4. A typical interface element.

$$\nabla \cdot \left[D_1(\nabla n_1^{(j+1)} + q_1 n_1^{(j+1)} \nabla \psi^{(j)}) \right] = 0, \quad \text{on} \quad \Omega^+, \tag{3.8}$$

$$n_1^{(j+1)} = g, \quad \text{on} \quad Dir(\partial\Omega^+), \tag{3.9}$$

$$D_1(\nabla n_1^{(j+1)} + q_1 n_1^{(j+1)} \nabla \psi^{(j)}) \cdot \mathbf{n}_\Gamma = 0, \quad \text{on} \quad \partial\Omega^+ - Dir(\partial\Omega^+). \tag{3.10}$$

Here, $Dir(\partial\Omega^+)$ represents the part of $\partial\Omega^+$ where Dirichlet boundary condition is imposed for n_1. Let us remark on the Dirichlet boundary condition (3.9) and Neumann boundary condition (3.10). It is assumed that there is little change in concentration in regions far enough away from the channel. Therefore, one may choose suitable regions on $\partial\Omega^+$ for the $Dir(\partial\Omega^+)$ so that the function g has little change on $Dir(\partial\Omega^+)$. On the other hand, zero Neumann boundary condition is applied on the solute-solvent interface region Γ, since it is natural to assume that there is no charge transfer between the protein wall and solute region. The diffusion coefficient D_1 is given by

$$D_1 = \begin{cases} D^{bulk_I}, & \text{on} \quad \text{Bulk region I} \\ D^{channel}, & \text{on} \quad \text{Channel} \\ D^{bulk_{II}}, & \text{on} \quad \text{Bulk region II.} \end{cases}$$

4. Numerical method

In this section, we develop a numerical method for PBNP system based on the formulation described in the previous section. For the PB equation, DB-IFEM is used to control the nonhomogeneous jumps arising from the regularization process. For the NP equation which can be convection dominated, we use a control volume method together with an upwinding concept.

4.1. DB-IFEM with consistency terms for PB equation

We provide a modified version of IFEM based on P_1-conforming FEM introduced in [40,31].

Let $\mathcal{T}_h$ be uniform triangulations of Ω which do not necessarily have to align with the interface. For example, we divide Ω by axi-parallel lines and then subdivide the subrectangles by diagonals. We denote $\mathcal{T}_h^*$ as the set of all triangle elements divided by the interface. We may assume that the interface intersects with the boundary of an element at most twice (see Fig. 4), which holds when the mesh size is sufficiently small. We denote S_Γ^h as the union of elements in $\mathcal{T}_h^*$. As noted earlier, we can choose ψ^* so that the support of ψ^* is S_Γ^h. Let T be any elements in $\mathcal{T}_h^*$. $S_h(T)$ denotes the space of standard linear functions on T which has degrees of freedom on each node of T. Suppose T is cut through edges e_1 and e_2 at points E_1 and E_2 by Γ. Let T^+ and T^- be two subregions of T separated by $\overline{E_1E_2}$.

We modify $\phi \in S_h(T)$ so that the new function $\widehat{\phi}$ is a piecewise linear on T having the same values at nodes and satisfy jump conditions. Let $L_j (j = 1, 2, 3)$ be the linear Lagrange nodal basis functions associated with the vertices $A_j (j = 1, 2, 3)$, i.e., $L_j(A_i) = \delta_{ij}$. Then the form of $\widehat{\phi}$ with nodal basis value $V_i = \phi(A_i)(i = 1, 2, 3)$ is following:

$$\widehat{\phi}(x, y) = \begin{cases} \widehat{\phi}^+ = c_1 L_1 + V_2 L_2 + V_3 L_3 & \text{if} \quad (x, y) \in T^+ \\ \widehat{\phi}^- = V_1 L_1 + c_2 L_2 + c_3 L_3 & \text{if} \quad (x, y) \in T^-, \end{cases}$$

where the coefficients are determined by the following two jump conditions,

$$\widehat{\phi}^+(E_i) = \widehat{\phi}^-(E_i), \qquad i = 1, 2 \tag{4.1a}$$

$$\epsilon^+ \nabla \widehat{\phi}^+ \cdot n_{\overline{E_1E_2}} = \epsilon^- \nabla \widehat{\phi}^- \cdot n_{\overline{E_1E_2}}. \tag{4.1b}$$

It is well known that the coefficients of $\widehat{\phi}$ are determined uniquely by (4.1a)-(4.1b) [39]. The space of these functions $\widehat{\phi}$ is

denoted by $\hat{S}_h(T)$. Now we define P_1-conforming based IFEM space $\widehat{S}_h(\Omega)$ as follows:

$$\widehat{S}_h(\Omega) := \begin{cases} \widehat{\phi}|_T \in S_h(T), & \text{if } T \text{ is a noninterface element,} \\ \widehat{\phi}|_T \in \widehat{S}_h(T), & \text{if } T \text{ is an interface element,} \\ \widehat{\phi}|_{T_1}(X) = \widehat{\phi}|_{T_2}(X), & \text{where } X \text{ is a common node of } T_1 \text{ and } T_2 \\ \widehat{\phi}|_T(X) = 0, & \text{where } X \text{ is a node on } \partial\Omega. \end{cases}$$

We consider a bilinear form $\widetilde{a}_h(\cdot,\cdot)$ on $H_h(\Omega) := H_0^1(\Omega) + \hat{S}_h(\Omega)$. In the early version of IFEM, there were cases when the order of accuracy deteriorates caused by inconsistency of the bilinear form [41].

$$a_h(\bar{\psi}, v) := \sum_{T\in\mathcal{T}_h} \left(\int_T \epsilon \nabla\bar{\psi}\cdot\nabla v d\mathbf{x} + \int_T c_{add}\bar{\psi} v d\mathbf{x} \right).$$

Hence we add the following additional consistency terms:

$$b(\bar{\psi}, v) := \sum_{e\in\mathcal{E}_h} \left(-\int_e \{\epsilon\nabla\bar{\psi}\cdot\mathbf{n}_e\}_e [v]_e ds - \int_e \{\epsilon\nabla v\cdot\mathbf{n}_e\}_e [\bar{\psi}]_e ds \right),$$

$$j(\bar{\psi}, v) := \sum_{e\in\mathcal{E}_h} \int_e \frac{\sigma}{h}[\bar{\psi}]_e [v]_e \, ds,$$

where $\mathcal{E}_h$ is a set of all edges of $\mathcal{T}_h$ and $\mathbf{n}_e$ is a fixed directional unit normal vector to each edge. Here, $\{v\}_e$ and $[v]_e$ are the average and jump of $v \in H_h(\Omega)$ on an edge $e \in \mathcal{E}_h$ respectively. This technique resembles that of discontinuous Galerkin method. Then we define a new bilinear form:

$$\widetilde{a}_h(\bar{\psi}, v) := a_h(\bar{\psi}, v) + b(\bar{\psi}, v) + j(\bar{\psi}, v). \tag{4.2}$$

In the same spirit, we have to consider the consistency terms arising from ψ^* in (3.7). Thus, we obtain the following: Find $\bar{\psi} \in H_h(\Omega)$ satisfying

$$\begin{aligned} \widetilde{a}_h(\bar{\psi}, v) =& < J_2, v >_\Gamma - (\epsilon\nabla\psi^*, \nabla v) - b(\psi^*, v) - j(\psi^*, v) \\ &+ \left(\gamma[q_1 n_1^{(j)} + q_2 n_{02} e^{-(q_2(\bar{\psi}^{(j-1)}+\psi^*)-U_2^{(j)})}] + c_{add}\bar{\psi}^{(j-1)}, v \right), \quad \forall v \in H_h(\Omega), \end{aligned} \tag{4.3}$$

where $(\cdot,\cdot)$ denotes the $L^2(\Omega)$ inner product and $<\cdot,\cdot>_\Gamma$ denotes the $L^2(\Gamma)$ inner product. We briefly explain how to discretize the discontinuous bubble function ψ^* introduced in [6]. First, we let ψ_h^* be an approximation to ψ^*. It is desirable that ψ_h^* vanishes at each vertex of T so that ψ_h^* does not affect the value of $\bar{\psi}$ at vertices. Hence, ψ_h^* is piecewise linear on T^+ and T^- and is defined by:

$$\psi_h^*(A_i) = 0, \quad i = 1,2,3, \tag{4.4a}$$

$$\left[\psi_h^*(E_i)\right]_{\overline{E_1E_2}} = J_1(E_i), \quad i = 1,2, \tag{4.4b}$$

$$\epsilon^- \frac{\partial\psi_h^*}{\partial\mathbf{n}_{\overline{E_1E_2}}} - \epsilon^+ \frac{\partial\psi_h^*}{\partial\mathbf{n}_{\overline{E_1E_2}}} = \frac{1}{|\overline{E_1E_2}|}\int_{\overline{E_1E_2}} J_2. \tag{4.4c}$$

We note that the right hand side of (4.4c) can be computed pointwise. However, the average over $\overline{E_1E_2}$ is more general when the function J_2 is defined only in weak sense.

Having constructed ψ_h^* (see Fig. 5), we discretize the variational form (4.3). We shall use the new bilinear form (4.2). Then, we define DB-IFEM with consistency terms: Find $\bar{\psi}_h \in \widehat{S}_h(\Omega)$ such that

$$\begin{aligned} \widetilde{a}_h(\bar{\psi}_h, v_h) =& < J_2, v_h >_\Gamma - (\epsilon\nabla\psi_h^*, \nabla v_h) - b(\psi_h^*, v_h) - j(\psi^*, v_h) \\ &+ \left(\gamma[q_1 n_1^{(j)} + q_2 n_{02} e^{-(q_2(\bar{\psi_h}^{(j-1)}+\psi_h^*)-U_2^{(j)})}] + c_{add}\bar{\psi_h}^{(j-1)}, v_h \right), \quad \forall v_h \in \widehat{S}_h(\Omega). \end{aligned} \tag{4.5}$$

Finally, the algorithm to obtain the numerical solution $\psi_h^{(j)}$ of PB equation is the following:

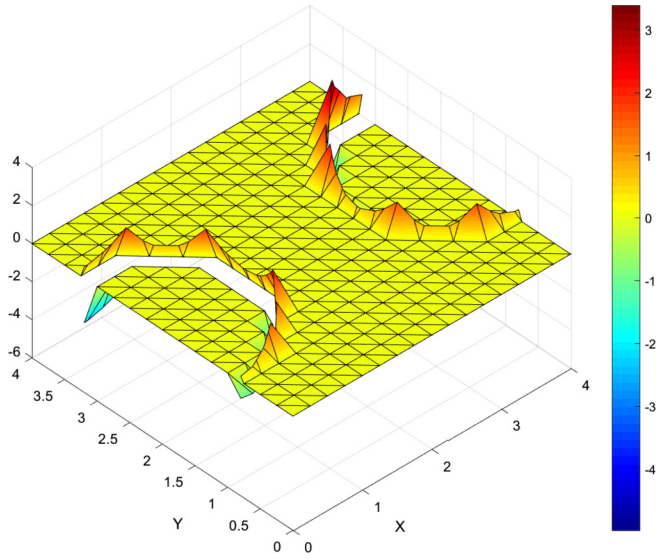

Fig. 5. The shape of S_Γ^h and the graph of the discretized bubble function.

1) Set $\bar{\psi}_h^{(j,0)} = \bar{\psi}_h^{(j-1)}$

2) For $n = 1, 2, \ldots$

Solve (4.5) with $\bar{\psi}^{(j-1)}$ replaced by $\bar{\psi}_h^{(j,n-1)}$ for $\bar{\psi}_h$

Set $\bar{\psi}_h^{(j,n)} = \bar{\psi}_h$

If $\|\bar{\psi}_h^{(j,n)} - \bar{\psi}_h^{(j,n-1)}\| < \text{tol}$ stop

End

3) $\bar{\psi}_h{}^{(j)} = \bar{\psi}_h^{(j,n)}$

4) $\psi_h^{(j)} = \bar{\psi}_h{}^{(j)} + \psi_h^* + \psi^s$.

Note that the numerical scheme for PB equation is given on structured grids. An advantage of structured grids is the applicability of fast solver such as multigrid method. For example, the multigrid solver for the PB equation developed by one of the authors in [35] can be applied to this case. We leave the development of the multigrid solver for the PBNP as a future work.

4.2. Control volume scheme for NP equation via upwinding concept

Once $\bar{\psi}_h^{(j)}$ is determined by the (4.5), the concentration variable is reconstructed by solving NP equation (3.8)-(3.10) using a control volume scheme [3,17,14,2]. We use usual P_1-conforming space for NP variable. Thus, the uniform grid $\mathcal{T}_h$ should be slightly refined near the solute-solvent interface. The refined mesh from $\mathcal{T}_h$ will be noted by $\mathcal{F}_h$, and the modification process is described below. First, noninterface elements in $\mathcal{T}_h$ do not need refinement, so naturally they belong to $\mathcal{F}_h$. Suppose that T is an interface element in $\mathcal{T}_h$ and that E_1 and E_2 are the points where the interface passes through the edge of T. By connecting E_1 and E_2, element T is divided into a triangle and a quadrilateral (see Fig. 6 (left)). Next, by cutting the quadrilateral into two triangles in such a way that the maximum angles of the resulting triangles decrease, T is finally divided into three sub-triangles (say T_1^s, T_2^s, and T_3^s). Then the refined triangles, T_1^s, T_2^s and T_3^s, belong to $\mathcal{F}_h$. By refining all the interface elements into small triangles in a similar way, $\mathcal{F}_h$ is obtained (Fig. 6 (middle)). Since the domain of concentration variable is Ω^+, we define a subset of $\mathcal{F}_h$ (Fig. 6 (right)),

$$\mathcal{F}_h^+ = \{T \in \mathcal{F}_h \,|\, T \subset \Omega^+\}.$$

To define the control volume methods for the concentration equation, new finite spaces are introduced. Firstly, $V_h(\Omega^+)$ denotes the P_1-conforming space on $\mathcal{F}_h^+$. Now we need to define a test function space. Given a vertex P in $\mathcal{F}_h^+$, consider the elements sharing P as a node $\{T_k\}_{k=1}^{N_p}$. Connecting the barycenters and edge midpoints, one obtains a dual volume T_P^* (see Fig. 7). Denoting the collection of such dual volume by $\mathcal{D}_h$, we define the test function space $W_h(\Omega^+)$ as

$$W_h(\Omega^+) = \{w \in L^2(\Omega^+) | \psi \text{ is piecewise constant on each dual volume } T_P^* \in \mathcal{D}_h\}.$$

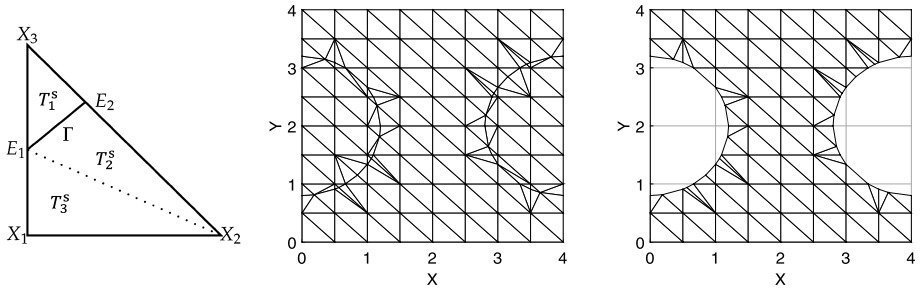

Fig. 6. Illustration of the triangulation of domain Ω^+ through refining of a uniform grid. Left figure shows a refinement process of a typical interface element T into three sub-triangles. Middle figure shows the resulting triangulation $\mathcal{F}_h$ and right figure shows its subset $\mathcal{F}_h^+$.

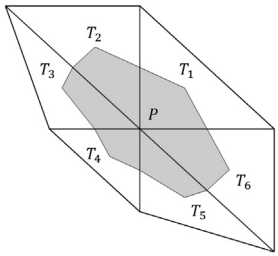

Fig. 7. Illustration of a dual volume associated with a node P (gray region). Connecting barycenters and edge midpoints of $T_1, T_2, \ldots, T_6$, dual volume T_P^* is obtained.

Given a vertex P_i in $\mathcal{F}_h^+$, let $w_i \in W_h(\Omega^+)$ be the function such that $w_i = 1$ on $T_{P_i}^*$ and $w_i = 0$ otherwise. It is easy to see that $\{w_i\}$ are basis functions of $W_h(\Omega^+)$. To obtain $n_{1,h}^{(j+1)}$, we multiply a test function $w_i \in W_h(\Omega^+)$ to (3.8) and integrate over $T_{P_i}^*$ as below

$$\int_{T_{P_i}^*} \nabla \cdot \left[D_1 (\nabla n_{1,h}^{(j+1)} + q_1 n_{1,h}^{(j+1)} \nabla (\bar{\psi}_h^{(j)} + \psi_h^*)) \right] \mathrm{d}\mathbf{x} = 0. \tag{4.6}$$

By integration by parts, (4.6) becomes

$$\int_{\partial T_{P_i}^*} \left[D_1 (\nabla n_{1,h}^{(j+1)} + q_1 n_{1,h}^{(j+1)} \nabla (\bar{\psi}_h^{(j)} + \psi_h^*)) \right] \cdot \mathbf{n} \mathrm{d}s = 0,$$

which is equivalent to

$$\sum_{k=1}^{N_P} \int_{\partial T_{P_i}^* \cap T_k} \left[D_1 (\nabla n_{1,h}^{(j+1)} + q_1 n_{1,h}^{(j+1)} \nabla (\bar{\psi}_h^{(j)} + \psi_h^*)) \right] \cdot \mathbf{n} \mathrm{d}s = 0. \tag{4.7}$$

Suppose P_ℓ is an adjacent node of P_i belonging to the element T_k with barycenter C_k. We denote by $M_{i\ell}$ the mid point of P_i and P_ℓ. Let us denote by $\gamma_{i\ell}^k$ the segment $\overline{M_{i\ell} C_k}$, whose outward normal vector is $\mathbf{n}_{i\ell}^k$. Then, (4.7) becomes

$$\sum_{k=1}^{N_P} \sum_{\ell = \ell_1^k, \ell_2^k} \int_{\gamma_{i\ell}^k} \left[D_1 (\nabla n_{1,h}^{(j+1)} + q_1 n_{1,h}^{(j+1)} \nabla (\bar{\psi}_h^{(j)} + \psi_h^*)) \right] \cdot \mathbf{n}_{i\ell}^k \mathrm{d}s = 0, \tag{4.8}$$

where $P_{\ell_1^k}$ and $P_{\ell_2^k}$ are two adjacent nodes of P_i, belonging to the element T_k (see Fig. 8). Since NP equation can be convection dominated, one needs to be careful to treat the convection term of (4.8) to avoid non-physical oscillations near the interface or boundary. Based on the usual upwinding concept, we replace the second term of (4.8) by

$$\sum_{k=1}^{N_P} \sum_{\ell = \ell_1^k, \ell_2^k} \int_{\gamma_{i\ell}^k} \left[D_1 q_1 n_{1,h}^* \nabla (\bar{\psi}_h^{(j)} + \psi_h^*)) \right] \cdot \mathbf{n}_{i\ell}^k \mathrm{d}s = 0,$$

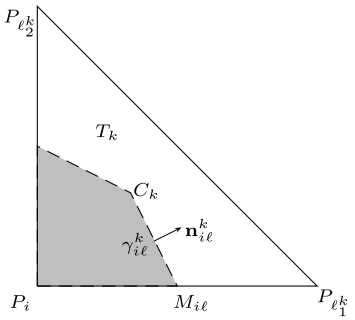

Fig. 8. Illustration of $\gamma_{i\ell}^k$ in T_k for $\ell = \ell_1^k$.

where

$$n_{1,h}^* = \begin{cases} n_{1,h}^{(j+1)}(P_i), & \text{if} \quad (\nabla(\bar{\psi}_h^{(j)} + \psi_h^*) \cdot \mathbf{n}_{i\ell}^k \geq 0 \\ n_{1,h}^{(j+1)}(P_\ell), & \text{if} \quad (\nabla(\bar{\psi}_h^{(j)} + \psi_h^*)) \cdot \mathbf{n}_{i\ell}^k < 0. \end{cases}$$

The final scheme for the NP equation is: Find $n_{1,h}^{(j+1)} \in V_h(\Omega^+)$ such that:

$$\sum_{k=1}^{N_P} \sum_{\ell=\ell_1^k, \ell_2^k} \int_{\gamma_{i\ell}^k} [D_1(\nabla n_{1,h}^{(j+1)} + q_1 n_{1,h}^* \nabla(\bar{\psi}_h^{(j)} + \psi_h^*))] \cdot \mathbf{n}_{i\ell}^k ds = 0,$$

for all nodes P_i of $\mathcal{F}_h^+$. Since we use an upwinding type scheme in P_1-conforming space, an expected optimal convergence rate for the concentration variable is $\mathcal{O}(h)$ for both L^2 and H^1-norms.

5. Numerical experiment

In this section, we provide some numerical experiments. In Section 5.1, we consider examples with analytic solutions and in Section 5.2, we consider an actual ion channel simulation. We report L^2 and H^1-errors and graphs of the numerical solutions. We observe optimal convergence for the concentration variable for all examples with analytic solutions. In Section 5.2, we show that our scheme reflects the effect on the distribution of electrons caused by locating the singular charge close to the interface. In all examples, the electrostatic potential variable is presented in $k_B T/e_c$ scale and the concentration variable is presented in molar scale. Also, we assume $q_1 = q_2 = 1$, $T = 25°\text{C}$ and $n_{02} = 1$ M.

5.1. Examples with analytic solutions

The experiments are conducted for problems with various pairs of dielectric coefficients in Example 5.1-5.3. Dirichlet boundary is imposed for both the electrostatic potential and concentration variables. We provide the numerical results in terms of L^2-error and piecewise H^1-error where the piecewise H^1-norm is defined as:

$$\|\psi\|_{1,h}^2 := \sum_{T \in \mathcal{T}_h} \|\psi\|_{\tilde{H}^1(T)}^2.$$

We let the domain $\Omega = [0,4]^2$ and we consider a uniform triangulation $\mathcal{T}_h$ consisting of right triangles whose size $h = 2^{-k}, k = 4, ..., 8$. The solvent-solute interface is given by following:

$$\Gamma = \begin{cases} x^2 + (y-2)^2 = 1.2^2, & x < 2 \\ (x-4)^2 + (y-2)^2 = 1.2^2, & x > 2. \end{cases}$$

Also, in the solvent domain, channel and bulk region I is separated by the line $y = 3$ and channel and bulk region II is separated by the line $y = 1$. The diffusion coefficient is determined by $D^{bulk_I} = 1.96 \times 10^{-5}$, $D^{bulk_{II}} = 2.03 \times 10^{-5}$ and $D^{channel} = 9.33 \times 10^{-7}$.

Example 5.1. We take $\epsilon^- = 1$ and $\epsilon^+ = 10$. The exact regular solution ψ^r is

$$\psi^r = \begin{cases} (x-2)^2 + (y-2)^2, & \text{on} \quad \Omega^-, \\ 0.64\exp(-x^2 - y^2), & \text{on} \quad \Omega^+, \end{cases}$$
$$n_1 = (x-2)^2 + (y-2)^2 + 3, \quad \text{on} \quad \Omega^+.$$

Table 1
The L^2 and H^1-errors of Example 5.1.

k	$\|\psi-\psi_h\|_{L_2(\Omega)}$	order	$\|\psi-\psi_h\|_{1,h}$	order	$\|n_1-n_{1,h}\|_{L_2(\Omega)}$	order	$\|n_1-n_{1,h}\|_{1,h}$	order
4	3.774×10^{-2}		4.553×10^{-1}		1.206×10^{-1}		7.215×10^{-1}	
5	9.661×10^{-3}	1.965	2.317×10^{-1}	0.974	5.793×10^{-2}	1.058	3.584×10^{-1}	1.009
6	3.279×10^{-3}	1.558	1.159×10^{-1}	0.999	2.926×10^{-2}	0.985	1.771×10^{-1}	1.016
7	1.530×10^{-3}	1.099	5.806×10^{-2}	0.997	1.461×10^{-2}	1.001	8.860×10^{-2}	0.999
8	7.928×10^{-4}	0.948	2.903×10^{-2}	0.999	7.326×10^{-3}	0.996	4.427×10^{-2}	1.001
9	4.076×10^{-4}	0.959	1.452×10^{-2}	0.999	3.671×10^{-3}	0.996	2.213×10^{-2}	1.000

Table 2
The L^2 and H^1-errors for the perturbed interface case in Example 5.1.

k	$\|\psi-\psi_h\|_{L_2(\Omega)}$	order	$\|\psi-\psi_h\|_{1,h}$	order	$\|n_1-n_{1,h}\|_{L_2(\Omega)}$	order	$\|n_1-n_{1,h}\|_{1,h}$	order
4	1.077×10^{0}		1.393×10^{0}		1.135×10^{-1}		7.191×10^{-1}	
5	6.570×10^{-1}	0.714	7.982×10^{-1}	0.803	5.419×10^{-2}	1.067	3.567×10^{-1}	1.011
6	3.026×10^{-1}	1.118	3.484×10^{-1}	1.196	2.853×10^{-2}	0.926	1.777×10^{-1}	1.005
7	1.156×10^{-1}	1.388	1.429×10^{-1}	1.285	1.450×10^{-2}	0.976	8.869×10^{-2}	1.003
8	2.828×10^{-2}	2.032	4.953×10^{-2}	1.529	7.291×10^{-3}	0.992	4.431×10^{-2}	1.001
9	8.140×10^{-3}	1.797	1.808×10^{-2}	1.454	3.657×10^{-3}	0.995	2.213×10^{-2}	1.002

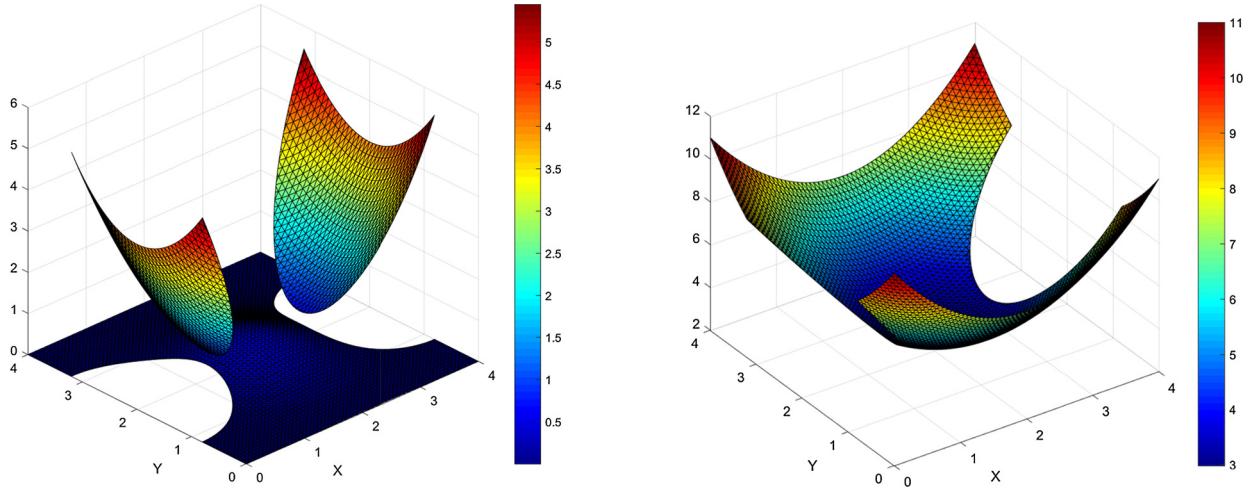

Fig. 9. The graph of numerical solution of ψ (left) and n_1 (right), $k=6$ (Example 5.1).

We report the L^2 and H^1-errors of Example 5.1 in Table 1. We observe that the convergence rates of concentration are optimal in L^2 and H^1-norms. However, we observe that the convergence rate of electrostatic potential converges to 1, which is optimal in this case. It is caused by the existence of concentration term in Poisson-Boltzmann distribution. The graphs are given in Fig. 9.

We consider a similar problem in the domain where the solvent-solute interface is perturbed by a sine function type high frequency graph. The L^2 and H^1-errors for this case is reported in Table 2 and the graphs are given in Fig. 10.

Example 5.2. We take $\epsilon^- = 1$ and $\epsilon^+ = 100$. The exact regular solution ψ^r is

$$\psi^r = \begin{cases} \sin(x+y-4), & \text{on} \quad \Omega^-, \\ \exp(\frac{x}{4}+\frac{y}{4}), & \text{on} \quad \Omega^+, \end{cases}$$
$$n_1 = \frac{xy}{4} + 5, \quad \text{on} \quad \Omega^+.$$

We report the L^2 and H^1-errors of Example 5.2 in Table 3. The graphs of numerical solutions are given in Fig. 11. The convergence rate of concentration is optimal in L^2 and H^1-norms. The convergence rate of electrostatic potential is $\mathcal{O}(h)$ for both L^2 and H^1-norms.

It seems the L^2 error of the electrostatic potential is suboptimal. This is caused by the concentration variable, not by the scheme. To see the optimality of our scheme, we fix the concentration variables and test the DB-IFEM scheme for the electrostatic potential alone in Table 4. We see that convergence rates for the potential are optimal.

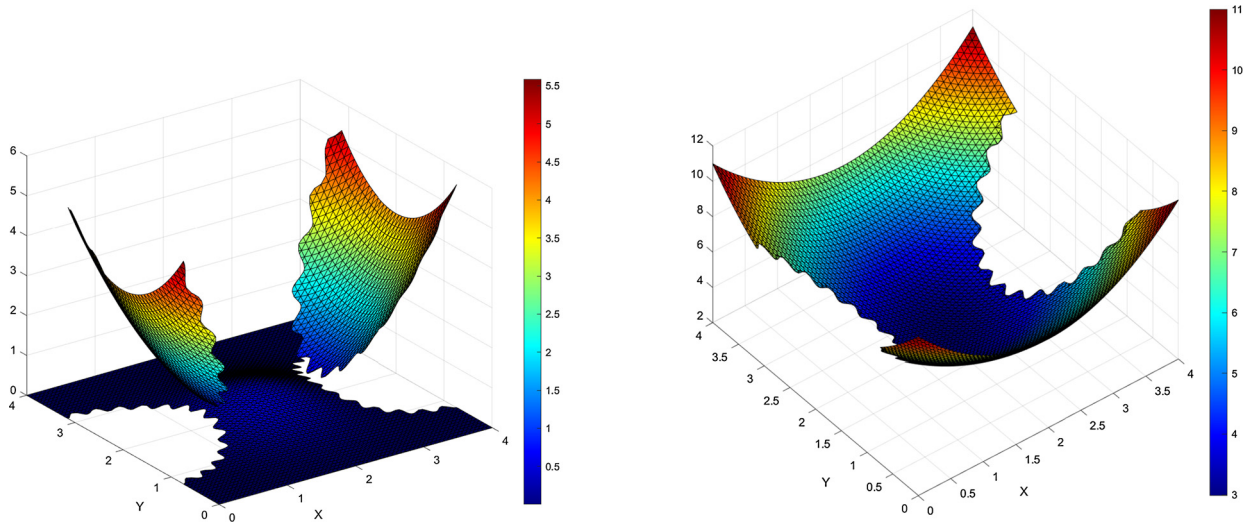

Fig. 10. The graph of ψ (left) and n_1 (right), for the perturbed interface case (Example 5.1).

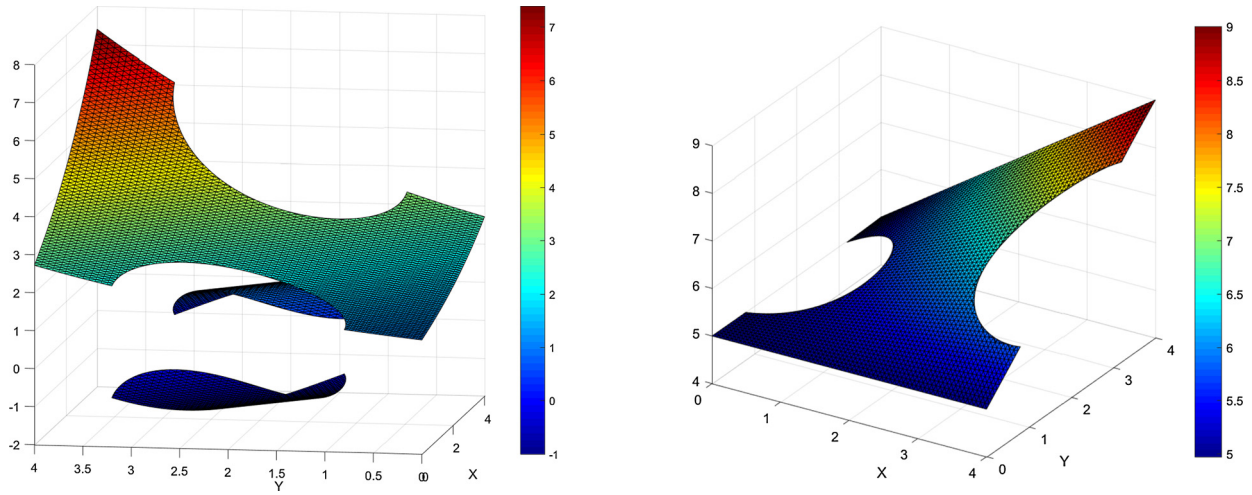

Fig. 11. The graph of numerical solution of ψ (left) and n_1 (right), $k = 6$ (Example 5.2).

Table 3
The L^2 and H^1-errors of Example 5.2.

k	$\|\psi - \psi_h\|_{L_2(\Omega)}$	order	$\|\psi - \psi_h\|_{1,h}$	order	$\|n_1 - n_{1,h}\|_{L_2(\Omega)}$	order	$\|n_1 - n_{1,h}\|_{1,h}$	order
4	1.005×10^{-2}		2.050×10^{-1}		1.151×10^{-1}		2.418×10^{-1}	
5	2.558×10^{-3}	1.973	9.947×10^{-2}	1.043	5.650×10^{-2}	1.026	1.220×10^{-1}	0.986
6	4.223×10^{-4}	2.599	4.800×10^{-2}	1.051	2.781×10^{-2}	1.022	5.807×10^{-2}	1.071
7	1.453×10^{-4}	1.538	2.390×10^{-2}	1.006	1.383×10^{-2}	1.007	2.854×10^{-2}	1.024
8	6.677×10^{-5}	1.122	1.188×10^{-2}	1.007	6.891×10^{-3}	1.004	1.410×10^{-2}	1.017
9	3.479×10^{-5}	0.940	5.932×10^{-3}	1.002	3.440×10^{-3}	1.002	7.027×10^{-3}	1.004

Table 4
The L^2 and H^1-errors electrostatic potential with fixed (true) value of concentration in Example 5.2.

k	$\|\psi - \psi_h\|_{L_2(\Omega)}$	order	$\|\psi - \psi_h\|_{1,h}$	order
4	1.032×10^{-2}		2.051×10^{-1}	
5	2.645×10^{-3}	1.964	9.947×10^{-2}	1.044
6	4.578×10^{-4}	2.530	4.800×10^{-2}	1.051
7	1.168×10^{-4}	1.971	2.390×10^{-2}	1.006
8	2.767×10^{-5}	2.077	1.189×10^{-2}	1.007
9	6.810×10^{-6}	2.023	5.933×10^{-3}	1.003

Table 5
The L^2 and H^1-errors of Example 5.3.

k	$\|\psi - \psi_h\|_{L_2(\Omega)}$	order	$\|\psi - \psi_h\|_{1,h}$	order	$\|n_1 - n_{1,h}\|_{L_2(\Omega)}$	order	$\|n_1 - n_{1,h}\|_{1,h}$	order
4	4.000×10^{-2}		2.723×10^{-1}		3.786×10^{-2}		3.924×10^{-1}	
5	1.784×10^{-2}	1.164	1.411×10^{-1}	0.948	1.714×10^{-2}	1.143	1.866×10^{-1}	1.072
6	8.859×10^{-3}	1.010	7.172×10^{-2}	0.976	8.576×10^{-3}	0.999	9.073×10^{-2}	1.040
7	4.419×10^{-3}	1.003	3.609×10^{-2}	0.990	4.399×10^{-3}	0.963	4.473×10^{-2}	1.020
8	2.218×10^{-3}	0.994	1.810×10^{-2}	0.995	2.236×10^{-3}	0.976	2.221×10^{-2}	1.009
9	1.113×10^{-3}	0.995	9.066×10^{-3}	0.997	1.128×10^{-3}	0.986	1.105×10^{-2}	1.006

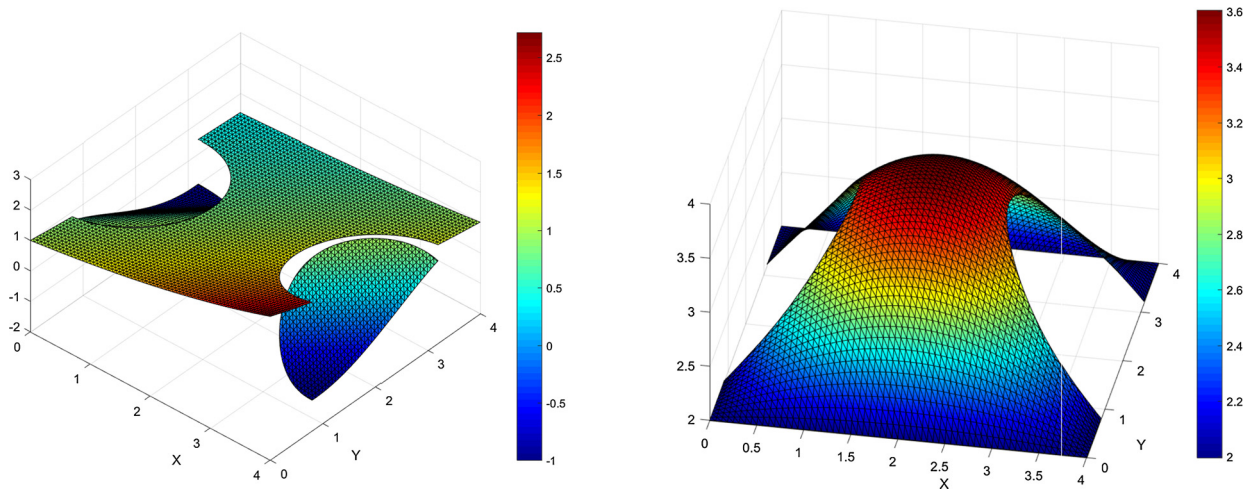

Fig. 12. The graph of numerical solution of ψ (left) and n_1 (right), $k = 6$ (Example 5.3).

Example 5.3. We take $\epsilon^- = 1$, $\epsilon^+ = 1$. The exact regular solution ψ^r is

$$\psi^r = \begin{cases} \cos(x-y), & \text{on} \quad \Omega^-, \\ \exp(\frac{x-y}{4}), & \text{on} \quad \Omega^+, \end{cases}$$
$$n_1 = 0.1x(x-4)y(y-4) + 2, \quad \text{on} \quad \Omega^+.$$

We report the L^2 and H^1-errors of Example 5.3 in Table 5. The graphs of numerical solutions are given in Fig. 12. We observe similar convergence rates as in Example 5.1 and Example 5.2.

5.2. Actual simulation

In this example, we consider an actual simulation of PBNP. First two experiments with one singular charge (Fig. 13 and 14) are given and then some experiments with multiple singular charges are given (Fig. 15). The purposes of different settings are 1) to show that our methods are robust regardless of the locations or the number of the charges, 2) to demonstrate the effects of singular charge on the distribution of electrons in the ion channel.

We let the domain $\Omega = [0, 4 \times 10^{-7}]^2$ in *cm*-unit. The solvent-solute interface is given by following:

$$\Gamma = \begin{cases} x^2 + (y - 2 \cdot 10^{-7})^2 = (1.2 \cdot 10^{-7})^2, & x < 2 \cdot 10^{-7} \\ (x - 4 \cdot 10^{-7})^2 + (y - 2 \cdot 10^{-7})^2 = (1.2 \cdot 10^{-7})^2, & x > 2 \cdot 10^{-7}. \end{cases}$$

Also, in the solvent domain, the channel and bulk region I is separated by the line $y = 1 \cdot 10^{-7}$ and the channel and bulk region II is separated by the line $y = 3 \cdot 10^{-7}$. Here, we take $\epsilon^- = 1$ and $\epsilon^+ = 10$. Also, we take $D^{bulk_I} = 1.96 \times 10^{-5}$ cm^2/s, $D^{bulk_{II}} = 2.03 \times 10^{-5}$ cm^2/s and $D^{channel} = 9.33 \times 10^{-7}$ cm^2/s. Let us describe the boundary condition. The following Dirichlet boundary condition is imposed for electrostatic potential variable, $\psi = 0$ on $y = 0$ and $\psi = 2$ on $y = 4 \times 10^{-7}$ while zero Neumann boundary condition is imposed on $x = 0$ and $x = 4 \times 10^{-7}$. For the concentration variable, Dirichlet boundary condition $n_1 = 2$ on $y = 0$ and $n_1 = 2$ on $y = 4 \times 10^{-7}$ is imposed and zero Neumann boundary condition is imposed on $x = 0$ and $x = 4 \times 10^{-7}$.

Let us examine the effects of singular charges in the solute domain especially when the charges are close to the solvent-solute interface. In this case, the electrostatic potential increases abruptly near the charge leading to a big gradient, which appears as the convection parameter in the concentration equation (see, eq. (3.8)-(3.10)). Hence the convection term dominates when the charge gets closer to the interface or the number of ions increases. However, in our numerical experiments,

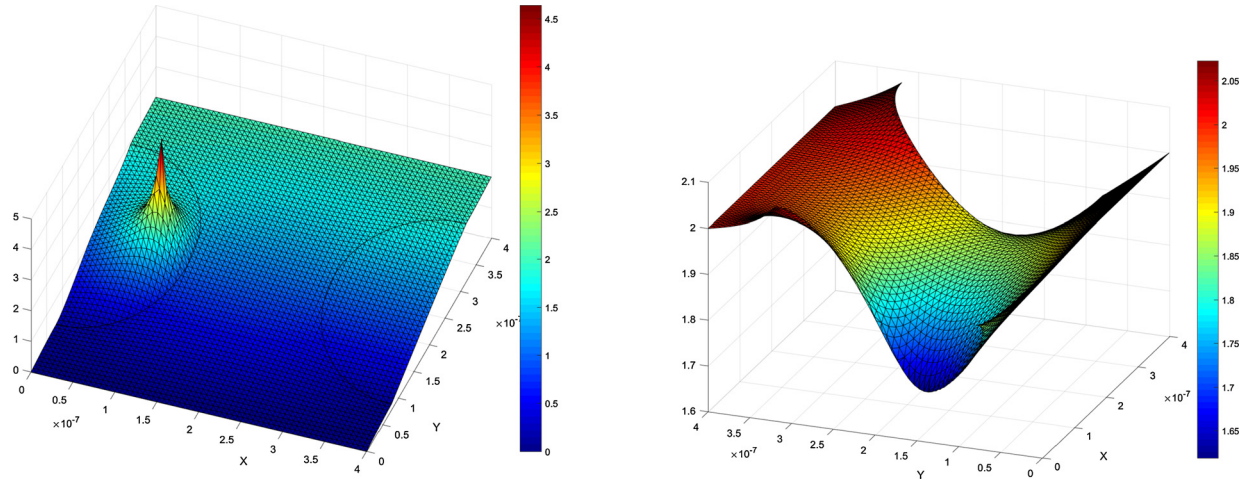

Fig. 13. The graph of electrostatic potential (left) and concentration (right) where h = $4\times10^{-7}/64$, the equation has the singularity at x = 10^{-7}, $y = 2\times10^{-7}$.

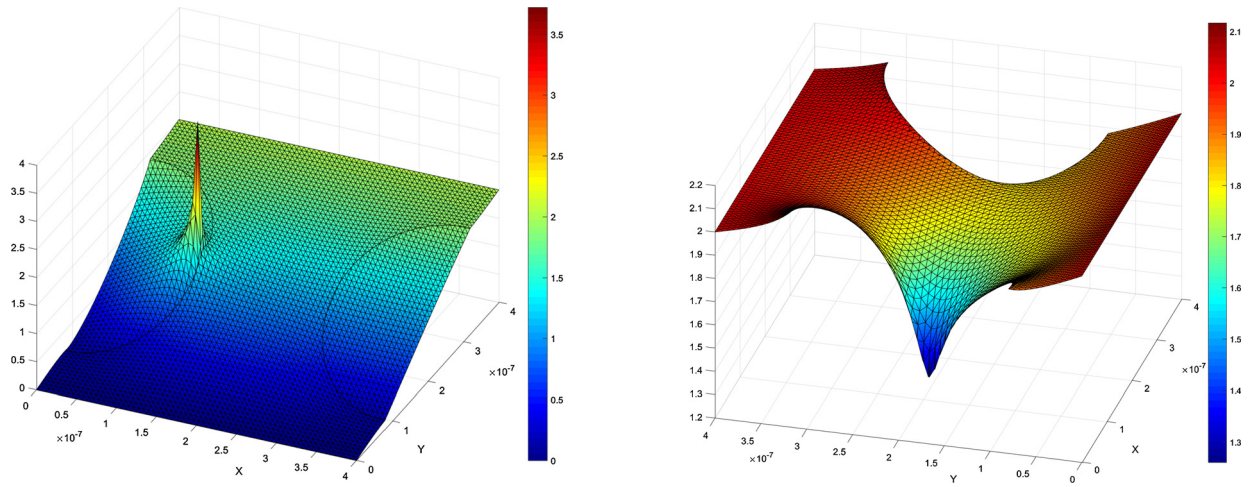

Fig. 14. The graph of electrostatic potential (left) and concentration (right) where h = $4\times10^{-7}/64$, the equation has the singularity at x = 1.13×10^{-7}, $y = 2\times10^{-7}$.

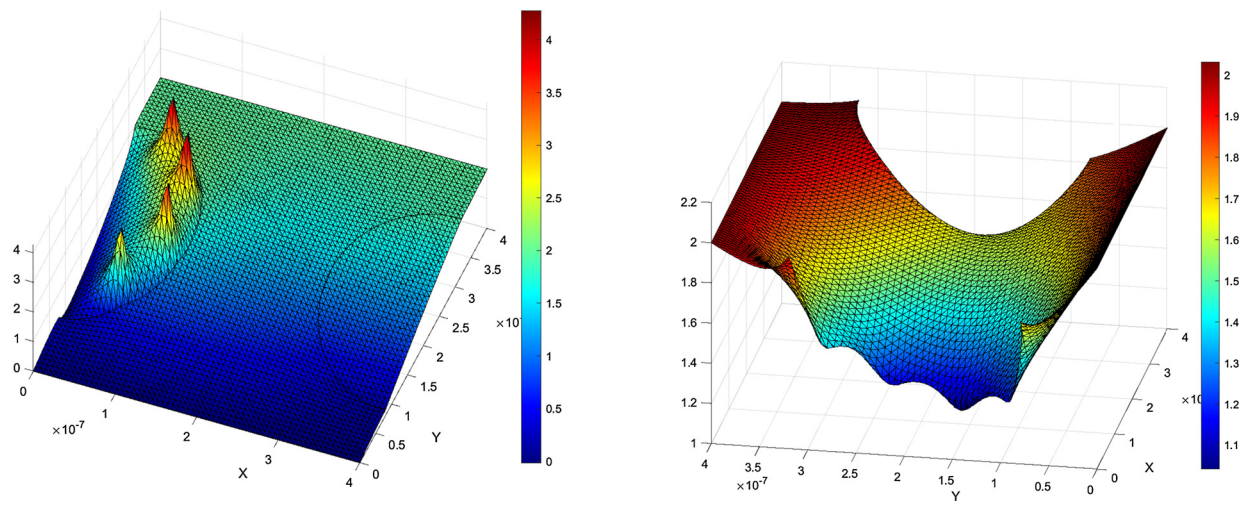

Fig. 15. The graph of electrostatic potential (left) and concentration (right) in the presence of the multiple charges.

the concentration and potential variables avoid any non-physical oscillations (see Fig. 14 for the close charge case and see Fig. 15 for the multiple charge case).

Also we can see our works reflect the effect of a singular charge has on the distribution of electrons, when the singular charge is close to the interface (Fig. 14). It is natural to expect that the concentration variable will change sharply near the interface as the singular charge gets closer to the interface, which coincides our numerical results. For example, when the singularity is close to the interface, the distribution of electrons near the interface goes down to 1.4 (Fig. 13), whereas that of electrons goes down to 1.7 when the singularity is far from the interface (Fig. 14).

6. Conclusion and future work

In this work, we introduced a new numerical method to solve the PBNP equation based on DB-IFEM. First, we regularized the solution of the PB equation. We introduced a DB to treat nonhomogeneous jumps and applied the linearization to the equation before discretization. Next, we defined a new variational form. Then, we discretized the DB and the bilinear form of the PB equation by adding consistency terms. Finally, we solved the discretized problem by IFEM. We repeated this process until the convergence of Gummel's iteration. We believe that this kind of scheme for removing the singularity of the PB equation and handling nonhomogeneous jumps of regular component is unique. In the numerical experiments, we observed optimal convergence rates of the concentration variable for all the examples.

We believe our scheme can be extended to the three dimensional cases following the three dimensional IFEM introduced in [22,21,44]. However, we must be careful on the construction of the bubble functions since the points of intersection may vary depending on the location of interface. We leave it as a future work.

CRediT authorship contribution statement

In Kwon: Writing – original draft. **Do Y. Kwak:** Conceptualization, Supervision. **Gwanghyun Jo:** Methodology.

Declaration of competing interest

The authors declare that they have no known competing financial interests or personal relationships that could have appeared to influence the work reported in this paper.

References

[1] F.G. Ball, J.A. Rice, Stochastic models for ion channels: introduction and bibliography, Math. Biosci. 112 (1992) 189–206.
[2] P. Bastian, Numerical Computation of Multiphase Flows in Porous Media, Habilitationsschrift Univeristät Kiel, 1999.
[3] J. Bear, Dynamics of Fluids in Porous Media, Elsevier, New York, 1972.
[4] T. Belytschko, T. Black, Elastic crack growth in finite elements with minimal remeshing, Int. J. Numer. Methods Eng. 45 (1999) 601–620.
[5] J. Cervera, B. Schiedt, P. Ramirez, A Poisson/Nernst-Planck model for ionic transport through synthetic conical nanopores, Europhys. Lett. 71 (2005) 35.
[6] K.S. Chang, D.Y. Kwak, Discontinuous bubble scheme for elliptic problems with jumps in the solution, Comput. Methods Appl. Mech. Eng. 200 (2011) 494–508.
[7] D. Chen, Z. Chen, C. Chen, W. Geng, G.-W. Wei, MIBPB: a software package for electrostatic analysis, J. Comput. Chem. 32 (2011) 756–770.
[8] L. Chen, M.J. Holst, J. Xu, The finite element approximation of the nonlinear Poisson–Boltzmann equation, SIAM J. Numer. Anal. 45 (2007) 2298–2320.
[9] I.-L. Chern, J.-G. Liu, W.-C. Wang, et al., Accurate evaluation of electrostatics for macromolecules in solution, Methods Appl. Anal. 10 (2003) 309–328.
[10] J. Chessa, T. Belytschko, An extended finite element method for two-phase fluids, J. Appl. Mech. 70 (2003) 10–17.
[11] S.H. Chou, D.Y. Kwak, K.T. Wee, Optimal convergence analysis of an immersed interface finite element method, Adv. Comput. Math. 33 (2010) 149–168.
[12] B. Corry, S. Kuyucak, S.-H. Chung, Tests of continuum theories as models of ion channels. II. Poisson–Nernst–Planck theory versus brownian dynamics, Biophys. J. 78 (2000) 2364–2381.
[13] H. Daiguji, Ion transport in nanofluidic channels, Chem. Soc. Rev. 39 (2010) 901–911.
[14] L.J. Durlofsky, Accuracy of mixed and control volume finite element approximations to Darcy velocity and related quantities, Water Resour. Res. 30 (1994) 965–973.
[15] B. Eisenberg, Proteins, channels and crowded ions, Biophys. Chem. 100 (2002) 507–517.
[16] W. Feng, X. He, Y. Lin, X. Zhang, Immersed finite element method for interface problems with algebraic multigrid solver, Commun. Comput. Phys. 15 (2014) 1045–1067.
[17] P.A. Forsyth, A control volume finite element approach to napl groundwater contamination, SIAM J. Sci. Stat. Comput. 12 (1991) 1029–1057.
[18] W. Geng, S. Yu, G. Wei, Treatment of charge singularities in implicit solvent models, J. Chem. Phys. 127 (2007) 114106.
[19] D. Gillespie, W. Nonner, R.S. Eisenberg, Coupling Poisson–Nernst–Planck and density functional theory to calculate ion flux, J. Phys. Condens. Matter 14 (2002) 12129.
[20] H.K. Gummel, A self-consistent iterative scheme for one-dimensional steady state transistor calculations, IEEE Trans. Electron Devices 11 (1964) 455–465.
[21] R. Guo, T. Lin, An immersed finite element method for elliptic interface problems in three dimensions, J. Comput. Phys. 414 (2020) 109478.
[22] D. Han, P. Wang, X. He, T. Lin, J. Wang, A 3D immersed finite element method with non-homogeneous interface flux jump for applications in particle-in-cell simulations of plasma–lunar surface interactions, J. Comput. Phys. 321 (2016) 965–980.
[23] U. Hollerbach, D.-P. Chen, R.S. Eisenberg, Two- and three-dimensional Poisson–Nernst–Planck simulations of current flow through gramicidin A, J. Sci. Comput. 16 (2001) 373–409.
[24] S. Jin, D.Y. Kwak, D. Kyeong, A consistent immersed finite element method for the interface elasticity problems, Adv. Math. Phys. 2016 (2016).
[25] G. Jo, D.Y. Kwak, A reduced Crouzeix–Raviart immersed finite element method for elasticity problems with interfaces, Comput. Methods Appl. Math. (2019).
[26] G. Jo, D.Y. Kwak, An IMPES scheme for a two-phase flow in heterogeneous porous media using a structured grid, Comput. Methods Appl. Mech. Eng. 317 (2017) 684–701.

[27] G. Jo, D.Y. Kwak, Geometric multigrid algorithms for elliptic interface problems using structured grids, Numer. Algorithms 81 (2019) 211–235.
[28] G. Jo, D.Y. Kwak, Recent development of immersed fem for elliptic and elastic interface problems, J. Korean Soc. Ind. Appl. Math. 23 (2019) 65–92.
[29] R. Karnik, R. Fan, M. Yue, D. Li, P. Yang, A. Majumdar, Electrostatic control of ions and molecules in nanofluidic transistors, Nano Lett. 5 (2005) 943–948.
[30] D.Y. Kwak, S. Jin, D. Kyeong, A stabilized P_1-nonconforming immersed finite element method for the interface elasticity problems, ESAIM: Math. Model. Numer. Anal. 51 (2017) 187–207.
[31] D.Y. Kwak, J. Lee, A modified P_1-immersed finite element method, Int. J. Pure Appl. Math. 104 (2015) 471–494.
[32] D.Y. Kwak, S. Lee, Y. Hyon, A new finite element for interface problems having Robin type jump, Int. J. Numer. Anal. Model. 14 (2017) 532–549.
[33] D.Y. Kwak, K.T. Wee, K.S. Chang, An analysis of a broken P_1-nonconforming finite element method for interface problems, SIAM J. Numer. Anal. 48 (2010) 2117–2134.
[34] I. Kwon, D.Y. Kwak, Discontinuous bubble immersed finite element method for Poisson-Boltzmann equation, Commun. Comput. Phys. 25 (2019) 928–946.
[35] I. Kwon, Discontinuous Bubble Immersed Finite Element Method for Poisson-Boltzmann Equation, Ph. D. dissertation, KAIST, 2020.
[36] D. Kyeong, et al., An immersed finite element method for the elasticity problems with displacement jump, Adv. Appl. Math. Mech. 9 (2017) 407–428.
[37] G. Legrain, N. Moes, E. Verron, Stress analysis around crack tips in finite strain problems using the extended finite element method, Int. J. Numer. Methods Eng. 63 (2005) 290–314.
[38] Z. Li, T. Lin, Y. Lin, R.C. Rogers, An immersed finite element space and its approximation capability, Numer. Methods Partial Differ. Equ. 20 (2004) 338–367.
[39] Z. Li, T. Lin, X. Wu, New Cartesian grid methods for interface problems using the finite element formulation, Numer. Math. 96 (2003) 61–98.
[40] T. Lin, Y. Lin, X. Zhang, Partially penalized immersed finite element methods for elliptic interface problems, SIAM J. Numer. Anal. 53 (2015) 1121–1144.
[41] T. Lin, Q. Yang, X. Zhang, A priori error estimates for some discontinuous Galerkin immersed finite element methods, J. Sci. Comput. 65 (2015) 875–894.
[42] B. Lu, Y.C. Zhou, G.A. Huber, S.D. Bond, M.J. Holst, J.A. McCammon, Electrodiffusion: a continuum modeling framework for biomolecular systems with realistic spatiotemporal resolution, J. Chem. Phys. 127 (2007) 135102.
[43] B. Lu, Y.C. Zhou, M.J. Holst, J.A. McCammon, Recent progress in numerical methods for the Poisson-Boltzmann equation in biophysical applications, Commun. Comput. Phys. 3 (2008) 973–1009.
[44] C. Lu, Z. Yang, J. Bai, Y. Cao, X. He, Three-dimensional immersed finite-element method for anisotropic magnetostatic/electrostatic interface problems with nonhomogeneous flux jump, Int. J. Numer. Methods Eng. 121 (2020) 2107–2127.
[45] J.W. Mayer, Ion implantation in semiconductors, in: 1973 International Electron Devices Meeting, IEEE, 1973, pp. 3–5.
[46] N. Moës, T. Belytschko, Extended finite element method for cohesive crack growth, Eng. Fract. Mech. 69 (2002) 813–833.
[47] N. Moës, J. Dolbow, T. Belytschko, A finite element method for crack growth without remeshing, Int. J. Numer. Methods Eng. 46 (1999) 131–150.
[48] A. Shestakov, J. Milovich, A. Noy, Solution of the nonlinear Poisson–Boltzmann equation using pseudo-transient continuation and the finite element method, J. Colloid Interface Sci. 247 (2002) 62–79.
[49] Q. Zheng, G.-W. Wei, Poisson–Boltzmann–Nernst–Planck model, J. Chem. Phys. 134 (2011) 194101.